Journal of Materials Chemistry A

Accepted Manuscript

ROYAL SOCIETY OF CHEMISTRY

www.rsc.org/materialsA

Journal Name

COMMUNICATION

[2,2]Paracyclophane Triarylamine-based Hole-Transporting Material for High Performance Perovskite Solar Cells

Received 00th January 20xx,
Accepted 00th January 20xx

DOI: 10.1039/x0xx00000x

www.rsc.org/

Sungmin Park,[‡a,b] Jin Hyuck Heo,[‡c] Cheol Hong Cheon,[b] Heesuk Kim,[a] Sang Hyuk Im,*[c] Hae Jung Son*[a]

We report the development of a novel hole transporting material (HTM), PCP-TPA, based on [2,2]paracyclophane. In comparison to the well-known HTM, spiro-OMeTAD, PCP-TPA could be prepared using a simple synthesis and showed a higher hole mobility due to effective intermolecular aggregation in the film state. When used as a HTM in perovskite solar cells, the power conversion efficiency reached 17.6%. PCP-TPA will potentially replace spiro-OMeTAD and advance the development of cost-effective and practical perovskite solar cells.

Solid-state organometallic halide perovskite (e.g., methylammonium lead halides $CH_3NH_3PbX_3$, where X = halogen) solar cells have gained recognition as the most promising low-cost photovoltaic technology since the first pioneering reports of Park *et al.*.[1] Perovskites characterized by the chemical formula ABX_3 (A ¼ CH_3NH_3 or $NHCHNH_3$, B ¼ Pb, and X ¼ Br, Cl, or I) have several advantageous properties, including high light absorption,[1,2] excellent ambipolar charge mobility,[3-5] and a small exciton binding energy,[6,7] which importantly contribute to the excellent performances of the perovskite solar cells. Recently, Jeon *et al.* reported the properties of highly efficient mesoscopic perovskite solar cells with >17% power conversion efficiencies (PCEs),[8] and the efficiencies have gradually approached the efficiencies of crystalline Si solar cells.[9] In addition to the photovoltaic performance, it is important that the power generation cost is lower than the corresponding costs of all other photovoltaic technologies to ensure competitiveness in the solar cell market. Processing costs can be reduced by developing low-temperature solution processes, such as spray-coating, spin-coating, slot-die coatings, and roll-to-roll coatings. Importantly, the material costs should be minimized by developing new cost-effective materials or simplifying the solar cell device architectures because the perovskite solar cells are typically constructed using multiple stacked materials, including transparent electrodes, electron conductors, perovskites, hole transporting materials, and metal electrodes.[1]

Among the materials used to fabricate perovskite solar cell devices, hole-transporting materials (HTMs) play a key role in enhancing the solar cell efficiency by inducing efficient hole transport and slowing electron–hole recombination.[10,11] The most widely used HTM, the spiro–OMeTAD (2,2′,7,7′-tetrakis[*N*,*N*-di-*p*-methoxyphenylamine]-9,9′-spirobifluorene), reproducibly performs well, irrespective of the perovskite solar cell device architecture (i.e., mesoscopic Al_2O_3/TiO_2 scaffolds[12] or planar heterojunction structures[9]) since it was developed as a HTM for use in solid-state dye-sensitized solar cells.[5 13] Despite its promising properties, the high cost of spiro-OMeTAD impedes the practical applications of highly efficient perovskite solar cells in the photovoltaic market because spiro-OMeTAD requires complicated multi-step synthesis approaches.[14] Novel polymeric HTMs have been developed, such as poly(3-hexylthiophene)(P3HT), poly[2,1,3-benzothiadiazole-4,7-diyl[4,4-bis(2-ethylhexyl)-4H-cyclopenta[2,1-b:3,4-*b*′]dithiophene-2,6-diyl]](PCPDTBT), and poly-triarylamine (PTAA)[4] and small molecular HTMs, such as the *N*,*N*-di-*p*-methoxyphenylamine-substituted pyrene derivatives,[15] 4-(4-phenyl-4-a-naphthyl-

[a] *Photoelectronic Hybrid Research Center, Korea Institute of Science and Technology, Seoul, Korea, E-mail: hjson@kist.re.kr*
[b] *Department of Chemistry, Korea University, Seoul, Republic of Korea*
[c] *Functional Crystallization Center (FCC), Department of Chemical Engineering, Kyung Hee University, Yongin-si, Gyeonggi-do, Republic of Korea, E-mail: imrom@khu.ac.kr*
[d] These authors contributed equally to this work.
† Electronic Supplementary Information (ESI) available. See
DOI: 10.1039/x0xx00000x

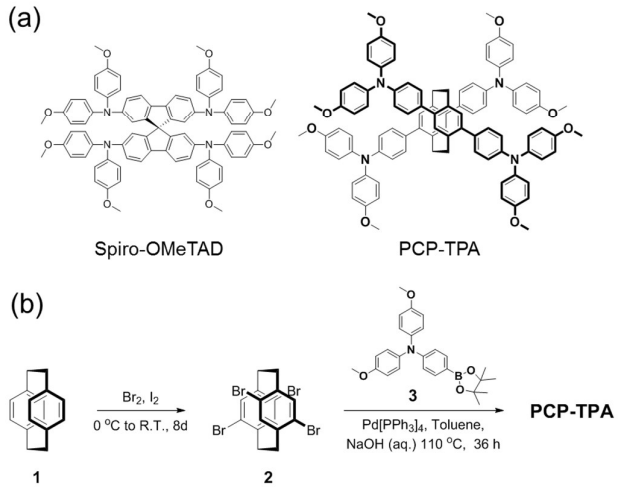

Fig. 1 (a) Chemical structures and (b) Synthetic routes of PCP-TPA.

butadienyl)-*N*,*N*-di(4-methoxyphenyl)-phenylamine,[16] and 2,5-bis(4,4′-bis(methoxyphenyl)aminophen-4′′-yl)-3,4-ethylenedioxythiophene[14], have been also synthesized. Although polymeric HTMs exhibit comparable device efficiencies in perovskite solar cells, they are far from practical use because their photovoltaic properties depend significantly on batch-to-batch variations in the molecular weights of the polymeric HTMs.[17] Small molecular HTMs are better for fabricating reproducible perovskite solar cells. Therefore, it is important to develop new small molecular HTMs that are inexpensive and perform better than spiro-OMeTAD.

We report the synthesis and photovoltaic properties of a novel small molecular HTM, PCP-TPA, a triphenyl amine-based compound that incorporates [2,2]paracyclophane as a core (see Fig. 1). PCP-TPA can be synthesized from the relatively inexpensive and commercially available [2,2]paracyclophane through several synthetic steps. thermore, PCP-TPA, which employs [2,2]paracyclophane, has structural features that are advantageous for efficient charge transport. (i) First, the cylindrical and rigid structure of the [2,2]paracyclophane framework promotes dense packing among the HTM molecules. (ii) At the same time, the three-dimensional structure of the molecule favors charge transport.[18,19] (iii) The extended π-conjugation in *N*,*N*,*N*′′,*N*′′-tetrakis(4-methoxyphenyl)-[1,1′:4′,1′′-terphenyl]-4,4′′-diamine (Ph-diTPA) enhances effective intermolecular interactions among neighboring molecules and thus, decreases the hopping distance.[20,21] Our results revealed that perovskite solar cells fabricated using PCP-TPA as an HTM displayed notably better performances with a PCE of 17.6% under AM 1.5 G illumination at 100 mW/cm^2. By contrast, the spiro-OMeTAD HTM showed a 15.4% PCE.

The procedures used to synthesize PCP-TPA are shown in Fig. 1(b), and and the experimental details are described in the Electronic Supporting Information (ESI). [2,2]Paracyclophane was brominated using Br_2/I_2, and then PCP-TPA was obtained by a Suzuki coupling reaction of the brominated [2,2]paracyclophane and 4-(4-methoxydiphenylamino)phenylboronic ester. The resulting compound PCP-TPA was characterized by $^1H/^{13}C$ NMR spectroscopy and mass spectrometry (see the ESI). The ^1H NMR spectrum showed two broad multiplets at δ = 3.40–3.55 and 2.72–2.85, corresponding to the protons at the ethano bridge, which were present in distinct chemical environments. The down-field peak corresponded to protons positioned closer to the triarylamine substitution, as shown in Figure S1. A singlet at δ = 3.79 ppm corresponded to the eight methoxy group protons. MALDI-TOF mass spectrum revealed peaks at m/z = 1420.409 and m/z = 710.253, which corresponded to molecular ion [M^+] and [M^{2+}], respectively, and further confirmed the chemical structure of PCP-TPA (Fig. S3). The thermal properties of PCP-TPA were studied by thermogravimetric analysis (TGA) and differential scanning calorimetry (DSC), both of which techniques were performed under a nitrogen atmosphere at a heating rate of 25 °C/min and 10°C/min for TGA and DSC, respectively. The TGA curves (Fig. S4(a)) showed that PCP-TPA had a similar thermal stability, with an onset decomposition temperature corresponding to a 5% weight loss (T_d) at 446.0°C, compared with spiro-OMeTAD, which had a T_d at 452.1°C.

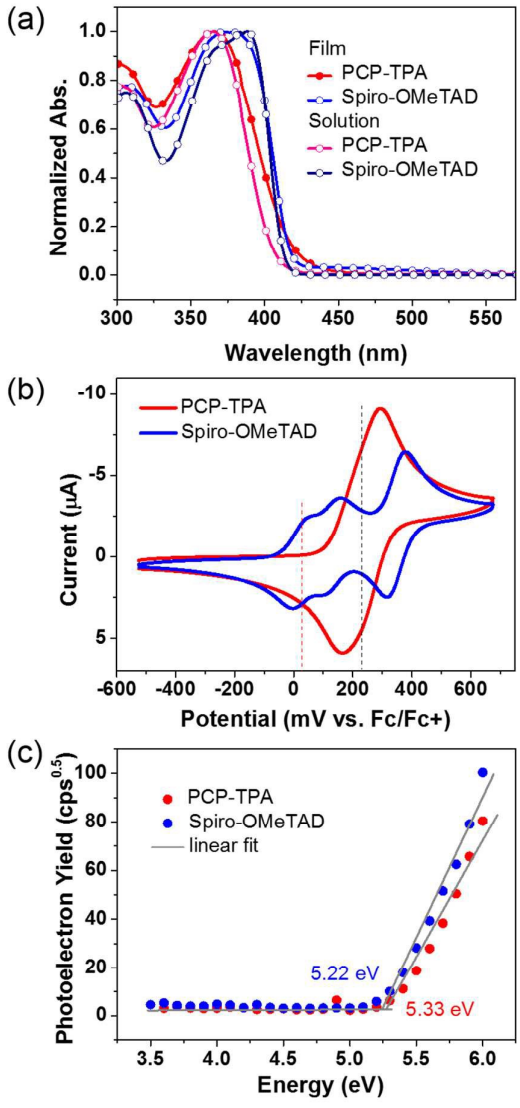

Fig. 2 UV-vis absorption spectra (a), cyclic voltammograms (b), and PESA spectra (c) of PCP-TPA and spiro-OMeTAD

Table 1. Optical and electrochemical properties of PCP-TPA and spiro-OMeTAD

HTM	Optical properties (solution (film))			Electrochemical properties		
	λ_{max} (nm)	λ_{em} [a] (nm)	E_g [b] (eV)	$E^{1/2}_{ox}$ [c] (V)	HOMO [d] (eV)	LUMO [e] (eV)
PCP-TPA	365 (366)	451 (465)	2.96	0.23	-5.33	-2.37
Spiro-OMeTAD	388 (372)	415 (427)	3.04	0.03	-5.13	-2.09

[a] Excitation at λ_{max}. [b] From the intersection of absorption and emission spectra. [c] CV measurements and referenced internally to ferrocene. [d] Calculated from the $E^{1/2}_{ox}$ of the respective redox waves; Fc/Fc+ was set to -5.1 eV vs. vacuum. [e] LUMO = HOMO + E_g.

The DSC results shown in Fig. S4(b) revealed that the glass transition temperature (T_g) in PCP-TPA (148.5°C) exceeded 123.4°C, the value obtained from spiro-OMeTAD, probably due to the improved molecular packing structure in PCP-TPA compared to that of spiro-OMeTAD. T_g is usually affected by the free volume,[22,23] which depends on the molecular packing density of the molecules. The UV-vis absorption properties of PCP-TPA were investigated, as shown in Fig. 2(a), and the characteristic data are listed in Table 1. In solution, PCP-TPA exhibited a strong absorption at 365 nm, representing a 23 nm blue shift relative to the absorption maximum obtained from spiro-OMeTAD at 388 nm. The absorption spectrum confirmed that PCP-TPA did not significantly absorb light in the visible region, indicating that the molecule would not compete significantly with the perovskite layer in a solar cell used for light harvesting. In a film, the onset point of the absorption spectrum of PCP-TPA was clearly red-shifted compared to that of the solution, whereas spiro-OMeTAD only displayed a minor change in the absorption onset. These results indicated that intermolecular aggregation among PCP-TPA molecules in the film was more effective than that of spiro-OMeTAD,[24] which is in good agreement with the DSC results obtained from the HTMs, as described above. The energy band gaps (E_gs) of PCP-TPA estimated from the absorption and emission spectra[25] (Fig. S5) were 2.96 eV, which was 0.08 eV lower than the 3.04 eV value obtained from spiro-OMeTAD. The electrochemical properties of the compound were studied using cyclic voltammetry (CV). Details are given in the ESI and a summary of the resulting data is given in Fig. 2(b) and Table 1. All oxidation curves were attributed the removal of electrons from the diarylamino centers.[26] In the cyclic voltammogram of PCP-TPA, the ~100 meV gap between the first and second peaks in the spiro-OMeTAD voltammograms disappeared, probably due to the increased N–N distance in PCP-TPA, which resulted in a decrease in the electronic interactions between the two redox active sites. A slight difference between the first oxidation potentials between PCP-TPA and spiro-OMeTAD; 0.23 V for PCP-TPA versus ferrocene/ferrocenium (Fc/Fc^+) was observed and this value was 0.20 V more positive than the value, 0.03 V, obtained from spiro-OMeTAD versus Fc/Fc^+. The limited electronic interactions between the two N atoms in PCP-TPA could also affect the first oxidation potential of the molecule. The highest occupied molecular orbital (HOMO) energy levels measured from the oxidation potentials in relation to Fc/Fc^+ and the HOMO (–5.33 eV) of PCP-TPA was deeper than that measured from spiro-OMeTAD (–5.13 eV). The HOMO energy levels of the HTMs, determined from thin films using photoelectron spectroscopy in air (PESA), showed a consistent result from the CV experiment; it was revealed that the HOMO of PCP-TPA (–5.36 eV) was lower than –5.22 eV for spiro-OMeTAD. The lowest unoccupied molecular orbitals (LUMO)s were calculated from the HOMO and E_g values and were found to be –2.37 eV and –2.09 eV for PCP-TPA and spiro-OMeTAD, respectively.

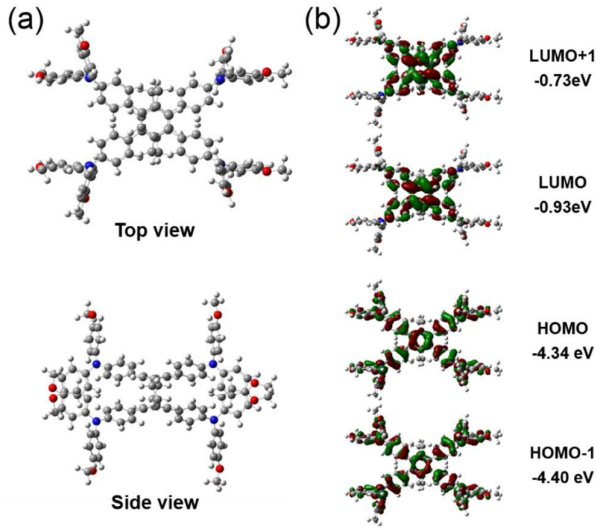

Fig. 3. Optimized molecular conformation (a) and HOMO/LUMO energy levels and frontier molecular orbitals (b) obtained from DFT calculations on PCP-TPA.

Density functional theory (DFT) calculations were performed to obtain the optimized geometries and electronic structures of PCP-TPA. Gaussian 09 was used to conduct the calculations based on the B3LYP hybrid functional and the 6-31G(d, p) basis set. As shown in Fig. 3(a), the Ph-diTPA units in the PCP-TPA molecule are positioned transannularly with spatial π-π interactions, which will favor intramolecular charge transport.[18] The cylindrical conformation of the PCP-TPA molecule will facilitate intermolecular π-π stacking in the film, and the multi-directional positioning of the triphenylamino groups will be favorable for intermolecular charge transport. Fig. 3(b) shows the frontier orbitals of the PCP-TPA; both of the HOMO and HOMO-1 were delocalized over the whole PCP-TPA molecule, which is probably because the Ph-diTPAs in the molecule were connected to each other with conjugation due to π-π interaction in the PCP core. It is expected that the oxidation processes involve the entire molecular framework of PCP-TPA. Interestingly, HOMO and HOMO-1 energy levels are very close to each other with an energy difference of 0.06 eV, which is not a much higher from the thermal energy at room temperature. Thus, HOMO/HOMO-1 may represent the two redox-active orbitals of the PCP-TPA molecule. The LUMO was mostly localized across the PCP core. The calculated HOMO and LUMO values were –4.34 eV and –0.93 eV, respectively and were lower than the corresponding energy values calculated for spiro-OMeTAD (HOMO: –4.21 eV, LUMO: –0.61 eV). The calculated band gap of PCP-TPA (ΔE = 3.41 eV) was 0.18 eV lower than the value calculated from spiro-OMeTAD (ΔE = 3.59 eV). These results were

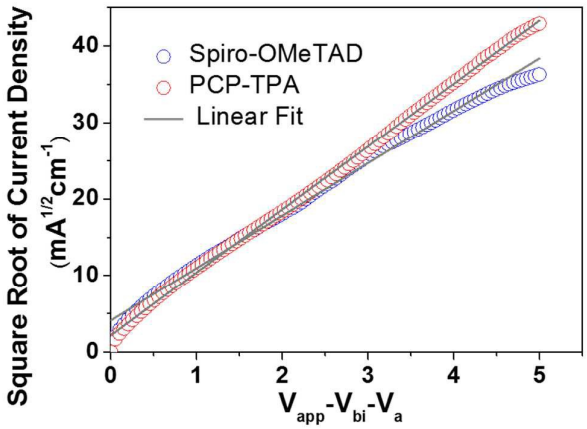

Fig. 4. *J* vs. *V* plots for the polymer films. The solid lines are fits of the data points.

consistent with the observations obtained from the CV and optical measurements.

The hole mobility values were measured using the space charge limited current (SCLC) method. Devices for measuring the mobility were prepared following a published procedure,[27,28] which involved preparing a spin-coated layer of the HTM on an ITO/PEDOT:PSS substrate, followed by evaporating a gold counter electrode. The closeness of the ITO and gold work functions to the HTM HOMO level and large mismatch to the HTM LUMO created a hole-only device from which the mobility could be determined. These samples contained *tert*-butyl pyridine (*t*BP) and lithium bis(trifluoromethylsulfonyl)imide salt (Li-TFSI) additives in concentrations that yielded the best solar cells. PCP-TPA showed a hole mobility value of 6.32×10^{-4} $cm^2/V{\cdot}s$, which exceeded the literature values reported for spiro-OMeTAD, $1–3.6 \times 10^{-4}$ $cm^2/V{\cdot}s$.[29-32] The detailed measurement conditions and averaged mobility values are descrbied in ESI. Our measurements revealed that the mobility in spiro-OMeTAD was 5.22×10^{-4} $cm^2/V{\cdot}s$ when measured using the same method. The higher mobility in the new HTM may be due to its advantageous molecular structure. The extended π-conjugation along with the rigid cylindrical structure favored intermolecular aggregation, which could facilitate intermolecular hopping processes.

Fig. 5(a) shows a schematic device architecture of a planar $MAPbI_3$ hybrid solar cell comprising FTO/TiO_2/$MAPbI_3$/HTM/Au. In a typical procedure for fabricating a planar $MAPbI_3$ hybrid solar cell, a TiO_2 electron conductor was deposited onto a cleaned FTO (F-doped tin oxide) substrate via spray-pyrolysis deposition using a 20 mM titanium diisopropoxide bis(acetylacetonate) solution at 450°C. A pinhole-free $MAPbI_3$ layer was then deposited onto the TiO_2/FTO substrate by spin-coating a 40 wt% $MAPbI_3$/DMF solution with a hydroiodic acid (HI) additive ($MAPbI_3$/DMF:HI = 1 mL:0.1 mL) at 3000 rpm for 200 s. The assembly was subsequently dried at 100 °C. (See the photographs in Fig. S6) An HTM layer was formed by spin-coating a spiro-OMeTAD or a PCP-TPA solution which including a Li-TFSI and 4-*tert*-butyl pyridine mixture dissolved in acetonitrile as an additive solution. Finally, an Au counter electrode was formed by thermal evaporation. Fig. 5(b) shows a representative SEM cross-sectional image of planar $MAPbI_3$ hybrid solar cells, revealing that the thickness of the TiO_2, $MAPbI_3$, HTM, and Au layers were 50 nm, 300 nm, 100 nm, and 70 nm, respectively. Figure 5(c) shows the corresponding energy band diagrams of each component, revealing that the electrons and holes generated in $MAPbI_3$ could be

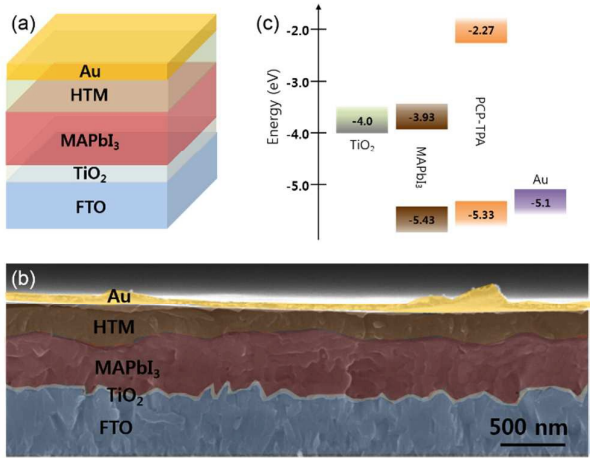

Fig. 5. Device architecture (a), the SEM cross-section image (b) and energy diagram (c) of perovskite solar cells prepared from PCP-TPA.

effectively transported to the electron conductor and HTM. Upon illumination with light, the $MAPbI_3$ layer absorbs the light and generates free electrons and holes or loosely bonded electron–hole pairs due to the small exciton binding energy of 30 meV,[6] which is comparable to the thermal energy at room temperature (1 kT = 25 meV, where k and T are the Boltzmann constant and absolute temperature, respectively). The generated electrons and holes are transported to a TiO_2 electron conductor and HTM, respectively. Fig. 6 shows the device performances of a planar $MAPbI_3$ hybrid solar cell prepared with different HTMs. The EQE spectra shown in Fig. 6(c) revealed that the planar $MAPbI_3$ hybrid solar cell prepared with the PCP-TPA HTM offered a better EQE value in the range of 350–800 nm compared to the spiro-OMeTAD sample. Here, we used the same thickness of $MAPbI_3$ films prepared using the same processing method so that the light harvesting efficiencies of both cells are almost identical to each other. It should be noted that only spiro-OMeTAD was replaced with the PCP-TPA HTM and the improved EQE was attributed to the improved properties of PCP-TPA HTM. Because the HOMO level of PCP-TPA (–5.33 eV) was 0.11 eV lower than that (–5.22 eV) of spiro-OMeTAD, the driving force for charge transfer from the perovskite to the HTM was predicted to be higher for spiro-OMeTAD than that for PCP-TPA. The enhanced photocurrent was, therefore, attributed to more efficient charge transport due to the higher hole mobility of PCP-TPA. Although the LUMO energy level of PCP-TPA was lower than the value obtained from spiro-OMeTAD, this energy level appeared to be sufficient to block electron transfer from the perovskite layer to the HTM and minimize charge recombination. The integrated EQE spectra of the spiro-OMeTAD and PCP-TPA samples were 20 mA/cm^2 and 21.2 mA/cm^2, respectively, in good agreement with the short circuit current density (J_{sc}) measured from each device, as shown in Fig. 6(a), Fig. 6(b) and Table 2. The photocurrent density–voltage (*J-V*) curves obtained from the planar $MAPbI_3$ hybrid solar cells prepared with different HTMs are shown in Fig. 6(a) and 6(b), and their photovoltaic properties summarized in Table 2. The planar $MAPbI_3$ hybrid solar cell, prepared with the spiro-OMeTAD HTM provided a PCE (η) of 15.1% under a forward scan condition with an open circuit voltage (V_{oc}) of 1.01 V, a short circuit current density (J_{sc}) of 20.5 mA/cm^2, and a fill factor (FF) of 73% and 15.7% η under a reverse scan condition with a V_{oc} of 1.01 V, a J_{sc} of 20.5 mA/cm^2, and a FF of 76%, thereby yielding an average PCE (η_{avg}) of 15.4% under 1 Sun conditions.

Table 2. Summary of photovoltaic properties of planar $MAPbI_3$ hybrid solar cells with different HTMs.

		V_{oc} (V)	J_{sc} (mA/cm^2)	FF (%)	η (%)	η_{avg}[a] (%)
PCP-TPA	Forward	1.04	22.0	76	17.4	17.6
	Reverse	1.04	22.0	78	17.8	
Spiro-OMeTAD	Forward	1.01	20.5	73	15.1	15.4
	Reverse	1.01	20.5	76	15.7	

[a] The average PCE values from the forward and reverse scans.

The planar $MAPbI_3$ hybrid solar cell prepared with the PCP-TPA HTM was characterized by a V_{oc} of 1.04 V, a J_{sc} of 22.0 mA/cm^2, and a FF of 76%, yielding 17.4% η under forward scan conditions and a V_{oc} of 1.04 V V_{oc}, a J_{sc} of 22.0 mA/cm^2, a FF of 78%, and 17.8% η under reverse scan conditions. The resulting η_{avg} under 1 Sun conditions was 17.6%. Fig. 6(d) shows histograms of the PCEs, indicating that the reproducibility of the performances was fairly high. The average PCE values were 15.8 ± 1.33% and 13.3 ± 1.32% for PCP-TPA and spiro-OMeTAD devices, respectively. The overall efficiency improvements arose from the increase in the J_{sc} from 20.5 to 22.0 mA/cm^2 and the slight enhancement in the FF value. The V_{oc} measured from PCP-TPA, which was 30 mV higher that the value measured from spiro-OMeTAD, was attributed to the lower HOMO energy level of PCP-TPA compared with spiro-OMeTAD. The improved photocurrent in the PCP-TPA device is most likely due to the higher hole transporting properties, which originated from more compact intermolecular aggregation among PCP-TPA molecules in the film.

Conclusions

In conclusion, we developed a hole transporting material that incorporated PCP as a core. This HTM was prepared using a PCP core which can be prepared using a simple synthetic process, thereby potentially reducing the manufacturing costs. The advantageous rigid and cylindrical structure of PCP-TPA enabled effective intermolecular aggregation in the film as simultaneously maintaining 3D directional transport pathways, which resulting in the increased charge carrier mobility. As a result, the perovskite solar cell fabricated using PCP-TPA displayed the higher photocurrent density compared with the value obtained from spiro-OMeTAD and thus, achieved a high solar cell efficiency of 17.6%. This cell efficiency is among the highest efficiencies yet reported for perovskite solar cells employing non-spiro-OMeTAD as a HTM. Our research results provide new guidelines for the development of HTMs and thus, the fabrication of efficient perovskite solar cells.

Notes and References

This work was supported by the Global Frontier R&D Program on Center for Multiscale Energy System funded by the National Research Foundation under the Ministry of Science, Korea Research Council of Fundamental Science and Technology (KRCF), Korea Institute of Science and Technology (KIST) for for Project No. 2E25392, the New and Renewable Energy Program of the Korea Institute of Energy Technology Evaluation and

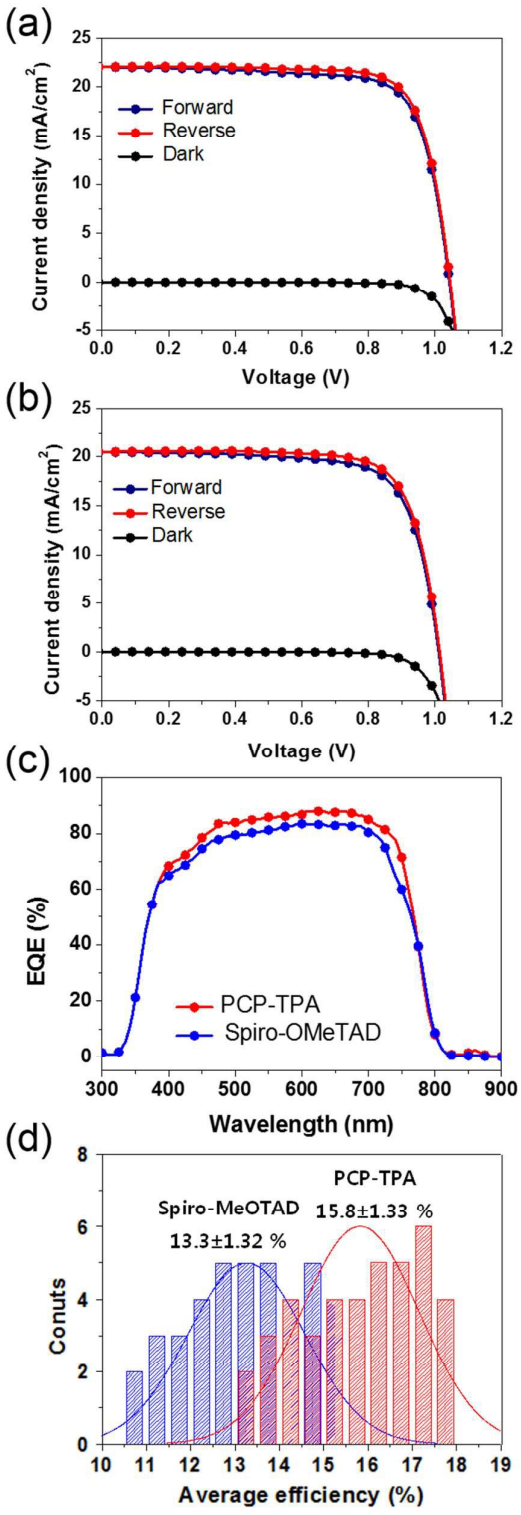

Fig. 6 Photovoltaic properties planar $MAPbI_3$ hybrid solar cells with PCP-TPA (a) and spiro-OMeTAD (b). (c) EQE spectra for PCP-TPA and spiro-OMeTAD-based solar cells. (d) Deviation of average power conversion efficiency of 40 spiro-OMeTAD and 40 PCP-TPA devices.

Planning (KETEP) grant funded by the Korea Goverment Ministry of Trade, Industry & Energy (MTIE) (20113030010030), and Mid-career Research Program (No.:NRF-2013R1A2A2A01067999) through the National Research Foundation of Korea (NRF) funded by the Ministry of Science, ICT & Future Planning.

1. H.-S. Kim, C.-R. Lee, J.-H. Im, K.-B. Lee, T. Moehl, A. Marchioro, S.-J. Moon, R. Humphry-Baker, J.-H. Yum, J. E. Moser, M. Gratzel and N.-G. Park, *Sci. Rep.*, 2012, **2**, 591-597.
2. N.-G. Park, *J. Phys. Chem. Lett.*, 2013, **4**, 2423-2429.
3. J. M. Ball, M. M. Lee, A. Hey and H. J. Snaith, *Energy. Environ. Sci.*, 2013, **6**, 1739-1743.
4. J. H. Heo, S. H. Im, J. H. Noh, T. N. Mandal, C.-S. Lim, J. A. Chang, Y. H. Lee, H.-j. Kim, A. Sarkar, K. NazeeruddinMd, M. Gratzel and S. I. Seok, *Nat. Photon*, 2013, **7**, 486-491.
5. S. Kazim, M. K. Nazeeruddin, M. Grätzel and S. Ahmad, *Angew. Chem. Int. Ed.*, 2014, **53**, 2812-2824.
6. S. D. Stranks, G. E. Eperon, G. Grancini, C. Menelaou, M. J. P. Alcocer, T. Leijtens, L. M. Herz, A. Petrozza and H. J. Snaith, *Science*, 2013, **342**, 341-344.
7. G. Xing, N. Mathews, S. Sun, S. S. Lim, Y. M. Lam, M. Grätzel, S. Mhaisalkar and T. C. Sum, *Science*, 2013, **342**, 344-347.
8. N. J. Jeon, J. H. Noh, W. S. Yang, Y. C. Kim, S. Ryu, J. Seo and S. I. Seok, *Nature*, 2015, **517**, 476-480.
9. M. Liu, M. B. Johnston and H. J. Snaith, *Nature*, 2013, **501**, 395-398.
10. N. J. Jeon, H. G. Lee, Y. C. Kim, J. Seo, J. H. Noh, J. Lee and S. I. Seok, *J. Am. Chem. Soc.*, 2014, **136**, 7837-7840.
11. J. Liu, Y. Wu, C. Qin, X. Yang, T. Yasuda, A. Islam, K. Zhang, W. Peng, W. Chen and L. Han, *Energy. Environ. Sci.*, 2014, **7**, 2963-2967.
12. M. M. Lee, J. Teuscher, T. Miyasaka, T. N. Murakami and H. J. Snaith, *Science*, 2012, **338**, 643-647.
13. U. Bach, D. Lupo, P. Comte, J. E. Moser, F. Weissortel, J. Salbeck, H. Spreitzer and M. Gratzel, *Nature*, 1998, **395**, 583-585.
14. H. Li, K. Fu, A. Hagfeldt, M. Grätzel, S. G. Mhaisalkar and A. C. Grimsdale, *Angew. Chem. Int. Ed.*, 2014, **53**, 4085-4088.
15. N. J. Jeon, J. Lee, J. H. Noh, M. K. Nazeeruddin, M. Grätzel and S. I. Seok, *J. Am. Chem. Soc.*, 2013, **135**, 19087-19090.
16. S. Lv, L. Han, J. Xiao, L. Zhu, J. Shi, H. Wei, Y. Xu, J. Dong, X. Xu, D. Li, S. Wang, Y. Luo, Q. Meng and X. Li, *Chem. Commun.*, 2014, **50**, 6931-6934.
17. O. P. Lee, A. T. Yiu, P. M. Beaujuge, C. H. Woo, T. W. Holcombe, J. E. Millstone, J. D. Douglas, M. S. Chen and J. M. J. Fréchet, *Adv. Mater.*, 2011, **23**, 5359-5363.
18. B. König, B. Knieriem and A. D. Meijere, *Chem. Ber.*, 1993, **126**, 1643-1650.
19. S. Amthor and C. Lambert, *J. Phys. Chem. A*, 2006, **110**, 1177-1189.
20. S. T. Bromley, M. Mas-Torrent, P. Hadley and C. Rovira, *J. Am. Chem. Soc.*, 2004, **126**, 6544-6545.
21. Y. Geng, J. Wang, S. Wu, H. Li, F. Yu, G. Yang, H. Gao and Z. Su, *J. Mater. Chem.*, 2011, **21**, 134-143.
22. D. Turnbull and M. H. Cohen, *J. Chem. Phys*, 1961, **34**, 120-125.
23. M. H. Cohen and G. S. Grest, *Phys. Rev. B*, 1979, **20**, 1077-1098.
24. G. He, Z. Li, X. Wan, J. Zhou, G. Long, S. Zhang, M. Zhang and Y. Chen, *J. Mater. Chem. A*, 2013, **1**, 1801-1809.
25. A. Abate, M. Planells, D. J. Hollman, V. Barthi, S. Chand, H. J. Snaith and N. Robertson, *Phys. Chem. Chem. Phys.*, 2015, **17**, 2335-2338.
26. E. T. Seo, R. F. Nelson, J. M. Fritsch, L. S. Marcoux, D. W. Leedy and R. N. Adams, *J. Am. Chem. Soc.*, 1966, **88**, 3498-3503.
27. G. G. Malliaras, J. R. Salem, P. J. Brock and C. Scott, *Phys. Rev. B*, 1998, **58**, R13411-R13414.
28. C. Goh, R. J. Kline, M. D. McGehee, E. N. Kadnikova and J. M. J. Fréchet, *Appl. Phys. Lett.*, 2005, **86**, 122110.
29. D. Poplavskyy and J. Nelson, *J. Appl. Phys.*, 2003, **93**, 341-346.
30. T. Leijtens, I. K. Ding, T. Giovenzana, J. T. Bloking, M. D. McGehee and A. Sellinger, *ACS Nano*, 2012, **6**, 1455-1462.
31. T. Leijtens, J. Lim, J. Teuscher, T. Park and H. J. Snaith, *Adv. Mater.*, 2013, **25**, 3227-3233.
32. A. Abate, D. R. Staff, D. J. Hollman, H. J. Snaith and A. B. Walker, *Phys. Chem. Chem. Phys.*, 2014, **16**, 1132-1138.

Table of Contents Figure

We report a new hole transporting material (HTM) based on [2,2]Paracyclophane triarylamine. Due to the higher charge

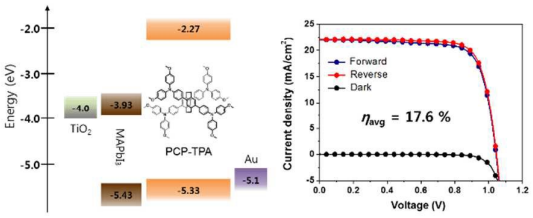

mobility compared with spiro-OMeTAD, the solar cell device incorporating the new HTM achieved a high photovoltaic performance with a PCE of 17.6%.